Biomaterials Translational

# Mechanically conditioned cell sheets cultured on thermo-responsive surfaces promote bone regeneration

*Gen Wang[#], Zhangqin Yuan[#], Li Yu[#], Yingkang Yu, Pinghui Zhou, Genglei Chu, Huan Wang, Qianping Guo, Caihong Zhu, Fengxuan Han, Song Chen[*], Bin Li[*]*

**Key Words:**
cell sheet; ECM production; mechanical loading; osteogenesis; PNIPAAm

## From the Contents




## ABSTRACT

*Cell sheet-based scaffold-free technology holds promise for tissue engineering applications and has been extensively explored during the past decades. However, efficient harvest and handling of cell sheets remain challenging, including insufficient extracellular matrix content and poor mechanical strength. Mechanical loading has been widely used to enhance extracellular matrix production in a variety of cell types. However, currently, there are no effective ways to apply mechanical loading to cell sheets. In this study, we prepared thermo-responsive elastomer substrates by grafting poly(N-isopropyl acrylamide) (PNIPAAm) to poly(dimethylsiloxane) (PDMS) surfaces. The effect of PNIPAAm grafting yields on cell behaviours was investigated to optimize surfaces suitable for cell sheet culturing and harvesting. Subsequently, MC3T3-E1 cells were cultured on the PDMS-g-PNIPAAm substrates under mechanical stimulation by cyclically stretching the substrates. Upon maturation, the cell sheets were harvested by lowering the temperature. We found that the extracellular matrix content and thickness of cell sheet were markedly elevated upon appropriate mechanical conditioning. Reverse transcription quantitative polymerase chain reaction and Western blot analyses further confirmed that the expression of osteogenic-specific genes and major matrix components were up-regulated. After implantation into the critical-sized calvarial defects of mice, the mechanically conditioned cell sheets significantly promoted new bone formation. Findings from this study reveal that thermo-responsive elastomer, together with mechanical conditioning, can potentially be applied to prepare high-quality cell sheets for bone tissue engineering.*


http://doi.org/10.12336/biomatertransl.2023.01.005

**How to cite this article:**
Wang, G.; Yuan, Z.; Yu, L.; Yu, Y.; Zhou, P.; Chu, G.; Wang, H.; Guo, Q.; Zhu, C.; Han, F.; Chen, S.; Li, B. Mechanically conditioned cell sheets cultured on thermo-responsive surfaces promote bone regeneration. *Biomater Transl.* **2023**, *4*(1), 27-40.

## Introduction

Bone tissue engineering aims to repair or replace impaired tissues by establishing three-dimensional complex with reconstructed shape, structure and/or functions mimicking those of original tissues.[1] Currently, typical protocols of bone tissue engineering involve *in vitro* seeding and culturing cells on designed scaffolds, followed by transplanting the engineered three-dimensional tissues into defect sites to restore the original tissues.[2, 3] Although many tissues have been successfully regenerated,[4-7] including eyes,[8] skin,[9, 10] cartilage,[11, 12] liver,[13, 14] heart[15] and muscle,[16, 17] the widespread application of tissue engineering is limited by the undesired side effects, including inflammation caused by the degradation of scaffolds, internal cell necrosis due to insufficient nutrient supply, and mismatch of cell proliferation and scaffold degradation.[18-20]

To meet these challenges, scaffold-free cell sheet engineering has been developed.[21] This approach overcomes a series of barriers within conventional tissue engineering,[22] including insufficient cell adhesion rate, potential inflammation, immune

response and reduced biological activity caused by scaffold materials.[23, 24] By now, functional cell sheets have been utilised to facilitate the regeneration of many soft tissues, including periodontal ligament,[25] blood vessels,[26] cornea[27] and myocardium.[28] To prepare the cell sheets, desired cells were cultured on a substrate to form a tissue-like sheet consisting of cells and their associated extracellular matrix (ECM), which were then harvested, assembled and transplanted. Traditionally, enzymes such as trypsin have been used to harvest cells from culture dishes. However, the hydrolysis process can impair different cell surface receptors, transporters and ECM.[29] In contrast to the harmful enzymatic treatment, recovering from the surface of thermally responsive polymers can retain the structure and function of cell sheets. Currently, substrates (e.g. tissue culture dish) functionalised with thermal responsive poly(N-isopropyl acrylamide) (PNIPAAm) were widely used for cell sheets culturing.[30-32] Above its low critical solution temperature (around 32°C), PNIPAAm is slightly hydrophobic and can support cell adherence, spreading and proliferation. While it becomes hydrophilic below its low critical solution temperature, forming a hydration layer between PNIPAAm and the cultured cells. Therefore, cell sheets cultured on PNIPAAm-functionalised substrates can be easily and integrally harvested by lowering the temperature, without disturbing cell-cell contact and association between cells and ECM.[33]

Although cell sheet culturing and harvesting have been greatly improved by utilizing temperature-sensitive polymers as the substrates, applying cell sheets to the repairing of hard tissues is rarely reported due to insufficient ECM content and poor mechanical strength.[34, 35] Recently, mechanical stimulation has been reported to play a key role in cell growth.[36-38] Numerous studies have shown that mechanical stimulation can regulate the behaviour of various cells, such as differentiation of stem cells,[39, 40] anabolic and biosynthetic activity of chondrocytes,[41, 42] progression of osteoarthritis[43] and osteogenic differentiation of human bone marrow-derived mesenchymal stem cells.[44] Appropriate loading and stimulation mimicking the internal cellular micro-environment have been demonstrated to promote cell proliferation, myofiber organization,[45-47] generation of ECM,[46] gene expression and bone formation.[48, 49] In addition, cyclic mechanical strain enhances the function and development of engineered tissues by improving the production of collagen and elastin.[50] Moreover, the mechanical properties of engineered tissues can also be improved by culturing under mechanical stimulation.[43] Therefore, cell sheets with enhanced thickness and mechanical properties obtained through appropriate cyclic mechanical stimulation possess great potential for bone tissue engineering applications.

In this study, we developed elastic and stretchable poly(dimethylsiloxane) (PDMS) substrates with grafted PNIPAAm surface for intact cell sheet harvesting, and appropriate mechanical stimulation was applied to obtain cell sheets with enhanced thickness and mechanical properties (**Figure 1**). Specifically, thermo-responsive elastomer substrates treated with surface $O_2$-plasma-ultraviolet (UV)-initiated polymerization were used as supporting substrates to culture cell sheets. Mechanical stimulation was further applied to the substrates to enhance the ECM production and osteogenic differentiation of cell sheets before they were subsequently implanted to the mouse calvarial defect sites. This technique can be applied to potential scaffold-free bone tissue engineering applications.

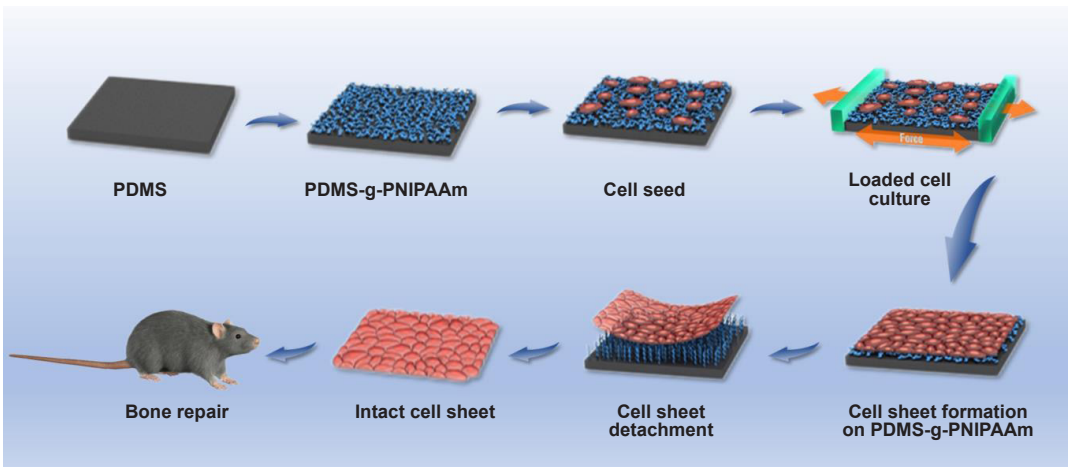


**Figure 1.** Schematic illustration of the preparation of cell sheets under mechanical stimulation and its implantation in a mouse calvarial defect model. Cells were cultured on the PDMS-g-PNIPAAm and then fixed in a loaded cell culture apparatus and subjected to cyclic mechanical stimulation to promote cell sheet formation. The harvested cell sheet was implanted into a calvarial defect of mouse for enhanced bone repair. PDMS-g-PNIPAAm: grafting polymerization of poly(N-isopropyl acrylamide) to poly(dimethylsiloxane).

***Corresponding authors:** Bin Li, binli@suda.edu.cn; Song Chen, chensong@suda.edu.cn.

#Author equally.

Orthopedic Institute, Department of Orthopaedic Surgery, The First Affiliated Hospital, Suzhou Medical College, Soochow University, Suzhou, Jiangsu Province, China

## Methods

### Preparation of thermo-responsive elastomer substrates

N-isopropyl acrylamide (NIPAAm) was purchased from J&K Scientific Ltd. (Beijing, China) and used as received PDMS (Dow Corning, Midland, MI, USA) substrates (1.5 mm thickness or specifically mentioned in the text) were prepared based on manufacturer's instruction. Briefly, PDMS precursor was mixed with curing agent (Dow Corning) with 10:1 ratio by weight, then degassed and cured in a polytetrafluoroethylene mold at 60°C overnight.

Cured PDMS substrates were fully rinsed with acetone (Yonghua Chemical Co., Ltd., Suzhou, China) and dried in vacuum oven (Shanghai Jing Hong Laboratory Instrument Co., Ltd., Shanghai, China) before grafting. The cleaned PDMS substrates were modified with oxygen plasma for 2 minutes, formed by a plasma cleaner (PDC-MG, Chengdu Mingheng Science&Thechnology Co., Ltd., Chengdu, China), to generate peroxide groups on PDMS substrates. Then the substrates were immediately immersed into NIPAAm aqueous solution with desired concentration and irradiated with UV lamp (500 W) to generate radicals to initiate grafting polymerization of PNIPAAm on PDMS substrates (PDMS-g-PNIPAAm). After 30 minutes, the substrates were cleaned with ultrapure water and dried with the blower. In this study, the polymerization was conducted with NIPAAm concentrations of 0.05 M, 0.1 M and 0.2 M to fabricate PDMS-g-PNIPAAm substrates with low, medium and high grafting yields, respectively (PDMS signify non-grafted PDMS substrate; gPDMS-L, gPDMS-M and gPDMS-H signify PDMS-g-PNIPAAm substrate with low, medium and high grafting yield, respectively).

### Attenuated total reflectance Fourier transform infrared spectroscopy analysis

PDMS-g-PNIPAAm surfaces were analysed using attenuated total reflectance Fourier transform infrared spectroscopy (Thermo Fisher Scientific, Waltham, MA, USA) in a wave number range of 650–4000 $cm^{-1}$. Thirty-six scans were performed for each sample and OMNIC 8.2 software (Thermo Fisher Scientific) was used to process the data. The absorbance ratio between the height of peaks at 1650 $cm^{-1}$ (PNIPAAm amide I) and 2962 $cm^{-1}$ (PDMS methyl absorbance) was calculated to determine the relative grafting yield, as previously described.[51]

### PDMS-g-PNIPAAm morphology observation

PDMS-g-PNIPAAm substrate with different grafting yields and pristine PDMS substrates were examined with a scanning electron microscope (SEM; Quanata250, FEI Company, Hillsboro, OR, USA). SEM imaging was performed with an acceleration voltage determined by smart SEM software (XT microscope Server, FEI Company). For analysis of the chemical composition on the substrates, energy dispersion spectrum (AMETEK, San Diego, CA, USA) was also performed. Atomic force microscopy (AFM; Bruker BioSpin, Billerica, MA, USA) imaging was conducted to analyze the surface morphology and surface roughness. AFM images were acquired by tapping mode in air with silicone tip cantilevers with imaging size of 10 μm × 10 μm scans at a scan rate of 0.2 Hz. The roughness of the samples was reported as root-mean-square roughness values.

### Contact angle measurements

Sessile drop method[52, 53] was used to analyze the static water contact angles on PDMS-g-PNIPAAm and pristine PDMS substrates using a KRUSS DSA25 contact angle equipment (KRÜSS, Hamburg, Germany). The substrates were rinsed with a large amount of 75% ethanol and dried in vacuum drying chamber before testing. ImageJ v1.8.0 software (National Institutes of Health, Bethesda, MD, USA)[54] was applied to determine contact angles.

To study the thermal responsiveness of PDMS-g-PNIPAAm samples, the water contact angles were measured in a temperature-controlled environmental chamber. Contact angles were taken at 4°C and 37°C. The chamber temperature was first equilibrated for 10 minutes and then a drop of water was dropped on the samples to measure the water contact angle. The values of contact angle were tested in at least three areas for each sample.

### Cell sheet culture

Mouse pre-osteoblast cells (MC3T3-E1, subclone 14, RRID: CVCL_0409) were bought from Cell Bank (Chinese Academy of Sciences, Shanghai, China) and cultured in alpha-minimum essential medium (HyClone, Logan, UT, USA) supplemented with 10% fetal bovine serum (HyClone) at 37°C and under a humidified 5% $CO_2$ atmosphere. The medium was replaced once every 2 days.

For cell sheet culturing, PDMS-g-PNIPAAm samples were first soaked in 75% ethanol for 2.5 hours and then exposed to fume hood ultraviolet light for 30 minutes. After sterilization, the samples were repeatedly cleaned with phosphate buffered saline (PBS) and coated with fibronectin by soaking in 20 μg/mL fibronectin (F8141-1MG, Sigma, St. Louis, MO, USA) in PBS overnight. The PDMS-g-PNIPAAm substrates were then placed in a PDMS cell culture dish fabricated according to our customised mold of similar cube box that was 6.0 cm in length, 3.0 cm wide and 2.0 cm high. MC3T3-E1 cells were inoculated on each substrate with a density of 360,000 cells (20,000 cells/$cm^2$). After the cells were passaged at 50% confluence, a group of samples was fixed in loaded cell culture system (Suzhou Haomian Precision Technology Co., Ltd., Suzhou, China) and further cultured under the loaded condition (loaded) for 3 days, while other samples were continuingly cultured under original static condition (static). A loaded cell culture system was utilised to apply dynamic mechanical stimulation to the cultured cell sheets by stretching the cell-attached elastic substrates cyclically. In this study, we applied uniaxial loading with 5% strain at a frequency of 0.5 Hz for 4 hours/day on cell sheets, according to previous studies.[55, 56] Cells under static condition were defined as the control group.

### Cell proliferation assay

Cell counting kit-8 (NCM Biotech, Suzhou, China) was utilised to analyse the proliferation of MC3T3-E1 cells cultured on PDMS-g-PNIPAAm substrate with the highest grafting yield after mechanical stimulation. Cells were cultured under both loaded and static conditions. After 1, 2, 3, 4 and 5 days, Cell

counting kit-8 was performed according to the instructions. The absorbance was measured spectrophotometrically using a microplate reader (BioTek, Winooski, VT, USA) at wavelength of 450 nm.

### Cell morphology observation

Cytoskeleton staining was applied to observe the morphology of cells cultured under different culture conditions. After culturing for 1, 3 and 5 days, MC3T3-E1 cells were fixed in 4% paraformaldehyde at 37°C for 30 minutes. The samples were then stained for actin with phalloidin (1:250, Cat# 40735ES75, Yeasen Biotechnology, Shanghai, China) and stained for nuclei with 4′,6-diamidino-2-phenylindole (1:1000, Beyotime, Shanghai, China). After staining, images of cytoskeleton staining were visualised via fluorescence microscopy (Zeiss Axiovert 200, Carl Zeiss Inc., Thornwood, NY, USA).

The same way was also performed after cell sheet detachment for observing the morphology change after detachment.

### Cell sheet harvesting

After 7 days of culturing, cell sheets were detached from the substrate and harvested by lowering the temperature from 37°C to 4°C in 10 minutes to initiate a thermal responsive change of PNIPAAm and detachment of cell sheets. The processes of cell sheet detachment and morphology change during detachment were imaged using a Nikon TMS inverted microscope (Japan) and recorded by a computer.

Cell viability in the cell sheet was determined using the live/dead viability cytotoxicity kit (C16702, Yeasen Biotechnology). After detachment, cell sheets were rinsed with PBS. The resultant cell sheets were incubated in the staining solution (2 μL Calcein-AM and 8 μL ethidium homodimer-1 in 2 mL PBS) for 1 hour. Fluorescence microscopy was used to image the cell sheets after detachment.

### Determination of the extracellular matrix production

Measurement of total proteins and DNA content of cell sheets was used to determine the ECM production. Briefly, cell sheets under different culture conditions were collected for extracting protein and DNA, respectively, after mechanical stimulation. Total proteins were extracted from cell sheets under different culture conditions using a tissue or cell total protein extraction kit (Sangon Biotech, Shanghai, China) according to the manufacturer's protocol. These proteins were quantified using a bicinchoninic acid protein assay kit (Beyotime). What's more, a cell/tissue DNA kit was used for DNA extraction (Yeasen Biotechnology) and concentration was measured using NanoDrop 2000 spectrophotometers (Thermo Fisher Scientific).

### Evaluation of cell sheets thickness

The thickness of cell sheets under different culture conditions was evaluated via section staining imaging and SEM imaging. The cell sheets were fixed in 4% paraformaldehyde for 30 minutes at room temperature and then dehydrated at 10%, 30%, 50%, 70%, 85%, 90%, and 100% alcohol for 10 minutes each time subsequently. The cell sheets were embedded in paraffin for hematoxylin and eosin (H&E) and Masson staining (Solarbio, Beijing, China), respectively. After staining, the cell sheet sections were imaged using a bright field microscope (Carl Zeiss Inc.). The images were analysed using ImageJ to determine the thickness of cell sheets. Each image of cell sheet section was measured at 200 points, and at least three samples per each test were taken for statistical analysis.

For SEM, after fixation and dehydration, the cell sheets were dried using a critical point dryer (Cat# CPD030, Leica, Wetzlar, Germany). The samples were then sputter coated with gold for 30 seconds using an Ion Sputter (SC7620, Quorum Technologies, Lewes, UK).

### Reverse transcription quantitative polymerase chain reaction

Reverse transcription quantitative polymerase chain reaction was tested to study the gene expression of type I collagen (Col I), Runt-related transcription factor 2 (Runx2) and osteopontin (OPN) from MC3T3-E1 cells that were cultured under different conditions. Total RNA was extracted using TRIzol reagent (Invitrogen, Carlsbad, CA, USA). Complementary DNA was synthesised from 1 μg of total RNA using IScript™ cDNA synthesis kit (Bio-Rad, Hercules, CA, USA). The housekeeping gene β-actin was used as an internal control and the relative changes in mRNA levels were analysed by the $2^{-\Delta\Delta CT}$ method. Sequences of primers for the target genes are listed in **Table 1**.[57]

**Table 1. Primers sequences used for reverse transcription quantitative polymerase chain reaction**

| Gene | Forward (5′–3′) | Reverse (5′–3′) |
|---|---|---|
| *Col I* | CCT AGC AAC ATG CCA ATC TTT ACA | TTG TCC ACG CGG TCC TCT |
| *Runx2* | CCA ACC CAC GAA TGC ACT ATC | TAG TGA GTG GTG GCG GAC ATA C |
| *OPN* | TGA GAC TGG CAG TGG TTT GC | CCA CTT TCA CCG GGA GAC A |
| *β-Actin* | TTC AAC ACC CCA GCC ATG T | GTG GTA CGA CCA GAG GCA TAC A |

Note: Col I: type I collagen; OPN: osteopontin; Runx2: Runt-related transcription factor 2.

### Western blot analysis

Western blotting was applied to quantify protein expression. Briefly, cells were rinsed with PBS and then lysed in extraction buffer and phenylmethylsulfonyl fluoride. Cell extracts were centrifuged at 4°C for 10 minutes, and the supernatants were then collected. The protein concentration of cells was measured using bicinchoninic acid protein quantification kit (Beyotime). The same amounts of the samples were separated using 10% sodium dodecyl sulfate-polyacrylamide gel electrophoresis (Beyotime), and then transferred to

nitrocellulose membranes (Beyotime). The membranes were blocked with 5% skim milk, using PBS with 0.05% Tween-20 for 2 hours. The membranes were then probed successively with Col I, Runx2, OPN and β-actin at 4°C overnight. The membranes were washed and then incubated with the respective horseradish peroxidase-conjugated secondary antibodies (LI-COR, Lincoln, NE, USA) for 1 hour at room temperature. Proteins were detected by autoradiography (Bio-Rad). The primary antibodies used in this study are listed in **Table 2**.

**Table 2. Antibodies for western blot analyses**

| Antibody | Species | Concentration | Catalog number | RRID number | Source |
|---|---|---|---|---|---|
| Col I | Mouse | 1:1000 | ab6308 | AB_305411 | Abcam, Cambridge, UK |
| Runx2 | Rabbit | 1:1000 | ab76956 | AB_156595 | Abcam, Cambridge, UK |
| OPN | Rabbit | 1:1000 | ab63856 | AB_1524127 | Abcam, Cambridge, UK |
| β-Actin | Mouse | 1:1000 | ab8226 | AB_306371 | Abcam, Cambridge, UK |
| Goat anti-rabbit horseradish peroxidase secondary antibody | Goat | 1:10000 | 926-80011 | AB_2721264 | LI-COR, Lincoln, NE, USA |
| Goat anti-mouse horseradish peroxidase secondary antibody | Goat | 1:10000 | 926-80010 | AB_2721263 | LI-COR, Lincoln, NE, USA |

Note: Col I: type I collagen; OPN: osteopontin; Runx2: Runt-related transcription factor 2.

### *In vivo* experiments

All procedures followed the National Research Council's Guide for the Care and Use of Laboratory Animals[58] and were approved by the Institutional Animal Care and Use Committee of Soochow University (ECSU-201700041) on August 1, 2017. Twenty-four male C57BL/6J mice (specific-pathogen-free level, 8 weeks old, 250 ± 5 g, Hangzhou Ziyuan Experimental Animal Technology Co., Ltd., license No. SCXK (Zhe) 2019-0004) were randomly divided into three groups (each group included eight samples). After mice were anaesthetized, a 4 mm diameter drill was then used to penetrate the left side of the entire calvarial to create defects. After filling the defect with cell sheets, the skin was tightly sutured. The skull samples were harvested at 4 and 8 weeks and fixed by 4% paraformaldehyde for 24 hours. The fixed mouse calvarial samples were analysed using a micro-computed tomography system (SkyScan 1176, SkyScan, Aartselaar, Belgium) at a voltage of 50 kV and an electric current of 50 μA. Three-dimensional reconstruction was performed using Mimics 15.0 software (Bruker BioSpin, Billerica, MA, USA) and calculating bone volume/tissue volume by using CTAn v1.12 software (Bruker BioSpin). All samples were immersed in decalcifying solution and the solution was changed every day for 2 weeks. These skull tissues were dehydrated with graded dehydration and embedded in paraffin before being sectioned into 6-μm thick slices. After deparaffinised and rehydrated, the slices were stained with H&E staining kits according to manufacturer's instructions.

### Statistical analysis

All data are expressed as the mean ± standard deviation (SD). Statistical analyses were performed by SPSS software (24.0, IBM Corp., Armonk, NY, USA) to determine the statistically significant differences among different groups. Statistical analyses including Student's *t*-test and one-way analysis of variance followed by Tukey's *post hoc* analysis were performed for two-group and multi-group comparisons, respectively. A significant difference was defined as a value of $P < 0.05$.

## Results

### Fabrication of PDMS-g-PNIPAAm substrates

PDMS-g-PNIPAAm substrates with different grafting yields were prepared by UV-initiated polymerization. This method is facile and the grafting yield of PNIPAAm can be easily controlled by adjusting the parameters like monomer concentration, UV radiation time, and temperature (**Additional Figure 1**). The surface morphology of PDMS-g-PNIPAAm substrate with different grafting yields was analysed using SEM and AFM (**Figure 2**). In general, the roughness of the surface increased after the modification. As shown in **Figure 2A** and **Additional Figure 2**, the pristine PDMS surface was clean and smooth, and the energy dispersion spectrum spectra revealed the peaks of carbon, oxygen and silicon. In comparison, the surfaces of PDMS, gPDMS-L, gPDMS-M and gPDMS-H substrate all showed uneven and wrinkled structures, and the structures became more evident with higher grafting yields. The gPDMS-H substrate showed the most wrinkled surface. The energy dispersion spectrum spectra showed nitrogen elements in addition to carbon, oxygen and silicon, demonstrating the successful grafting of PNIPAAm on the PDMS substrate. In addition, the SEM image of the cross section of the substrate (**Figure 2B**) showed that there was a clear thin layer of grafted PNIPAAm on the PDMS-g-PNIPAAm substrate, and the thickness increased with the increase of graft yields.

The surface morphology and roughness of the substrates were also analysed using AFM (**Figure 2C**). It was apparent that the PDMS-g-PNIPAAm substrate with higher grafting yield showed more uneven and corrugated structures. The surface roughness of PDMS, gPDMS-L, gPDMS-M and gPDMS-H substrate was measured to be 23.9 nm, 102 nm and 273 nm, respectively, which were evidently higher than 7.07 nm of pristine PDMS substrate.

Attenuated total reflectance Fourier transform infrared spectroscopy results showed the characteristic structures of the PDMS-g-PNIPAAm substrate with different grafting yields. As shown in **Figure 2D**, attenuated total reflectance

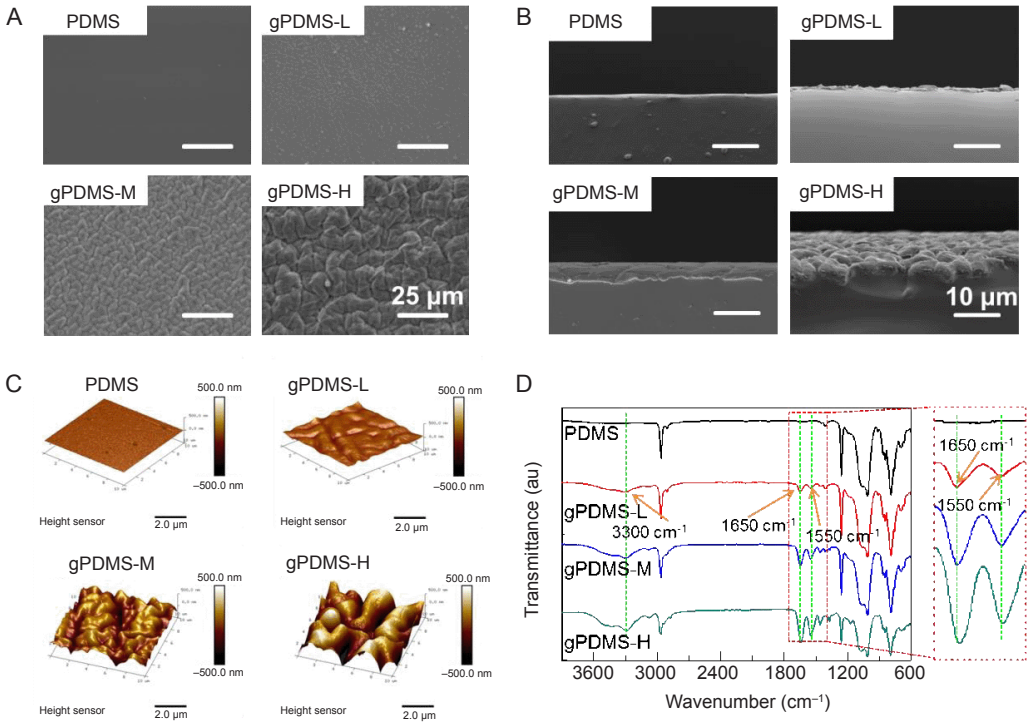


**Figure 2.** Microstructure of non-grafted PDMS substrate and PDMS-g-PNIPAAm substrate with different grafting yields. (A–D) SEM images (A), SEM images of the cross section (B), AFM images (C), and ATR-FTIR spectra (D) of the surfaces of PDMS, gPDMS-L, gPDMS-M and gPDMS-H substrates ($n \geq 3$). Scale bars: 25 μm (A), 10 μm (B), 2.5 μm (C). gPDMS-L, gPDMS-M and gPDMS-H indicate PDMS-g-PNIPAAm substrate with low, medium and high grafting yield, respectively. AFM: atomic force microscopy; ATR-FTIR: attenuated total reflectance Fourier transform infrared spectroscopy; au: arbitrary unit; PDMS: poly(N-isopropyl acrylamide); PDMS-g-PNIPAAm: grafting polymerization of poly(N-isopropyl acrylamide) to poly(dimethylsiloxane); SEM: scanning electron microscope.

Fourier transform infrared spectroscopy spectra of PDMS-g-PNIPAAm substrate with different grafting yields all revealed the presence of two new strong absorbance peaks at 1550 $cm^{-1}$ and 1650 $cm^{-1}$. The former can be assigned to the C=O stretching vibration of an amide group, while the latter to N–H deforming vibration of the amide group. Also, a broad peak appears at ~3300 $cm^{-1}$ that can be attributed to the N–H stretching vibration.[31, 59] These results demonstrated that the PNIPAAm has been successfully grafted on the surface of PDMS substrate. Moreover, it was observed that the height of peaks at 1550 $cm^{-1}$, 1650 $cm^{-1}$ and 3300 $cm^{-1}$ increased in accordance with increasing grafting yields, indicating more PNIPAAm was grafted on PDMS substrates with higher monomer concentration during polymerization.

### The detachment of cell sheets from PDMS-g-PNIPAAm substrates

The MC3T3-E1 cells were cultured at 37°C and detached at 4°C, therefore, the water contact angles of PDMS-g-PNIPAAm substrates were measured at 4°C and 37°C to evaluate their thermal response. The PDMS was hydrophobic, with water contact angles around 110° at 4°C and 37°C (**Figure 3A** and **B**). With PNIPAAm grafted, the PDMS-g-PNIPAAm substrates showed lower water contact angles (70°) than pristine PDMS at 37°C and the contact angles significantly decreased from 70° (hydrophobic) to 50° (hydrophilic) when lowering the temperature to 4°C. For PDMS-g-PNIPAAm substrates with high grafting yield, the most significant change of contact angle was observed, indicating their most evident thermal responsiveness, which makes them the most suitable for cell sheet detachment.

Subsequently, the detachment of cell sheets from PDMS-g-PNIPAAm substrate with different grafting yields was investigated (**Figure 3C**). The cell sheets began to detach by folding gradually from the edge of the substrate to the intermediate region, and continued to take place over time. The grafting facilitates the detachment of the cell sheets, as shown in **Figure 3C**, the substrate with the highest grafting yield detached much faster in comparison to other groups. The cell sheet on the PDMS-g-PNIPAAm substrate with the highest grafting yield finally migrated out of the view of microscope after 18 minutes. Then cell sheet was utterly detached and intact cell sheet could be obtained after 30 minutes. By contrast, the cell sheet remained firmly attached to PDMS substrate throughout the process. For PDMS-g-PNIPAAm substrates with low and medium grafting yields, effective detachment of cell sheets was not observed and intact cell sheets could not be harvested. The results indicated that the PDMS-g-PNIPAAm substrates with high grafting yield are most suitable for cell sheet detachment, therefore are selected for the following studies.

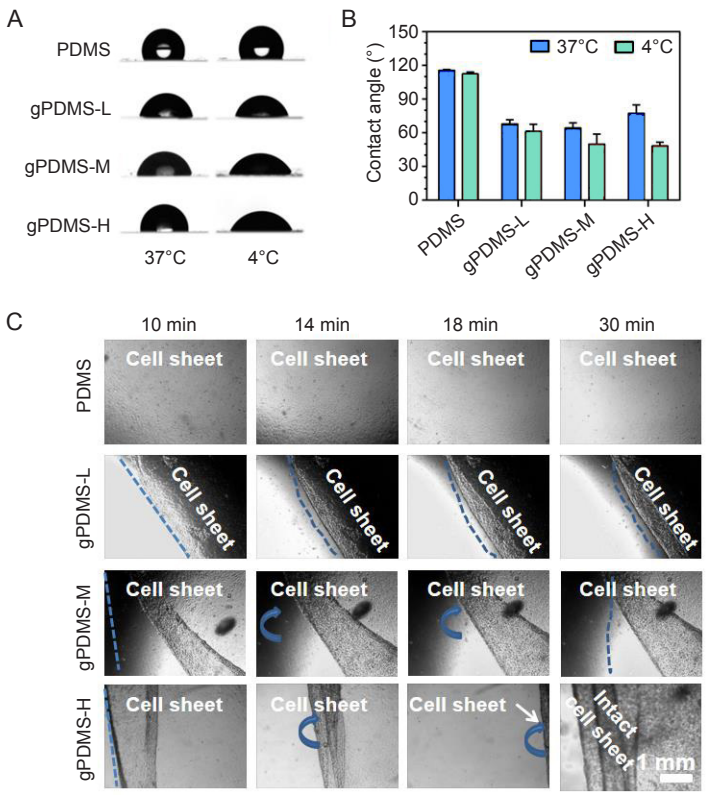


**Figure 3.** Temperature sensitivity of PDMS-g-PNIPAAm substrates. (A, B) The images of water contact angle (A) and water contact angle measured (B) on PDMS, gPDMS-L, gPDMS-M and gPDMS-H substrates with different grafting yields at 37°C and 4°C. Data are expressed as the mean ± SD ($n \geq 3$). (C) Detachment of cell sheets from the PDMS, gPDMS-L, gPDMS-M and gPDMS-H substrates after incubating at 4°C for 10, 14, 18 and 30 minutes. Blue dotted lines indicate the dividing line between the adhesion area and the detachment area of the cell sheet. Blue arrows indicate the direction of the detachment of the cell sheet. Scale bar: 1 mm . gPDMS-L, gPDMS-M and gPDMS-H indicate PDMS-g-PNIPAAm substrate with low, medium and high grafting yield, respectively. PDMS: poly(N-isopropyl acrylamide); PDMS-g-PNIPAAm: grafting polymerization of poly(N-isopropyl acrylamide) to poly(dimethylsiloxane).

**Cell sheets culture under mechanical conditioning**

MC3T3-E1 cells were cultured on PDMS-g-PNIPAAm substrates with high grafting yield to study the effect of mechanical stimulation on cell growth. **Figure 4A** showed the cell proliferation results at 1, 2, 3, 4, 5, 6 and 7 days obtained by cell counting kit-8 assay. Compared with the static group, the group with mechanical stimulation demonstrated higher optical density values, indicating enhanced proliferation under loaded condition. Cytoskeletal staining images showed that cells were able to adhere and proliferate well under both static and loaded conditions (**Figure 4B**).

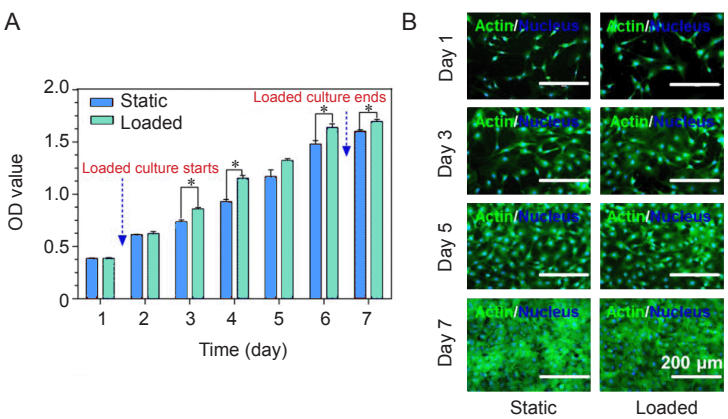


**Figure 4.** Loaded culture of cell sheets. (A) Cell proliferation under static or loaded conditions. Data are expressed as the mean ± SD ($n = 3$). *$P < 0.05$ (Student's *t*-test). (B) F-actin staining (green) of MC3T3-E1 cells under static or loaded conditions. Scale bars: 200 μm. OD: optical density.

**The detachment of cell sheets after loaded culture**

After mechanical stimulation, cell sheet detachment in both groups was studied. Intact cell sheets could be harvested in loaded group by lowering the temperature from 37°C to 4°C (**Figure 5A**). With the increase of time, the cell sheet gradually detached from the surface. The complete detachment time of the cell sheet in loaded group was slightly longer (~45 minutes) than that of static group, which might be attributed to enhanced thickness and strength due to mechanical stimulation. Cytoskeletal staining images showed the morphologies of cell sheets, before and after detachment. Before detachment, cells adhered to the substrate with flat and spread shape, and mutual extrusion were found to overlap (**Figure 5B**). Upon detachment, the shape of cells changed to spherical or ovoid due to loss of adhesion sites. Live/dead staining was conducted to study the cell viability (**Figure 5C**). The images showed that nearly all cells were dyed green both before and after detachment, indicating the viability of cells after detachment.

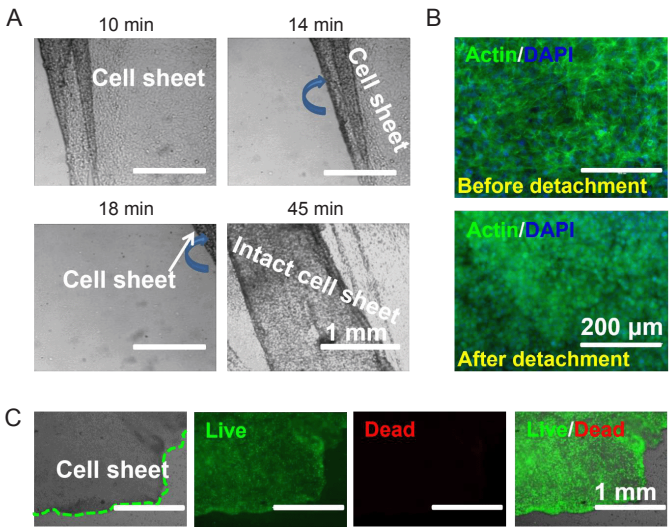


**Figure 5.** Cell sheets detachment after mechanical stimulation ($n$ = 3). (A) Detachment of cell sheets from the PDMS-g-PNIPAAm surface of high grafting yield after incubation at 4°C for 10, 14, 18 and 45 minutes. Blue arrows indicate the direction of the detachment of the cell sheet. (B) F-actin staining (green) of cell sheets before and after detachment. (C) Live/dead staining of cell sheets after detachment. The cell sheets were cultured under loaded condition to confluence. Green dotted lines indicate the dividing line between the cell sheet and the blank area. Scale bars: 1 mm (A, C), 200 μm (B). PDMS-g-PNIPAAm: grafting polymerization of poly(N-isopropyl acrylamide) to poly(dimethylsiloxane).

**Effect of mechanical stimulation on ECM production of cell sheets**

To determine if mechanical stimulation can promote ECM production, we characterised the thickness of the cell sheets cultured under static and loaded conditions. Cytoskeleton staining images showed that cells were uniformly dispersed within the cell sheet under both static and loaded conditions (**Figure 6A**), and no significant difference was observed between the groups. Under H&E staining, the thickness of cell sheets in loaded group is significantly larger than static group (**Figure 6B** and **C**). Masson staining revealed that the thickness of cell sheets under loaded condition was thicker than that under static condition (**Additional Figure 3**). The same result can also be observed in the SEM images. Furthermore, cell sheets obtained from loaded group showed more cell-to-cell junction and ECM content than static group (**Figure 6D**). Moreover, the ratio between total protein and total DNA of loaded group was also higher than static group, suggesting more ECM content density in loaded group (**Figure 6E–G**).

**Effect of mechanical stimulation on osteogenic differentiation**

The expression of osteogenic-specific genes (*Col I*, *Runx2*, and *OPN*) in cell sheets was examined using reverse transcription quantitative polymerase chain reaction (**Figure 7A–C**). The results showed that at 3 days, the expression of *Col I* and *Runx2* was higher in the loaded group than the static group, while the expression of *OPN* has no difference. The reason is that *Col I* and *Runx2* are mainly expressed during early osteogenesis, while *OPN* is generally expressed during late osteogenesis.[60] After culturing for 7 days, all the genes were expressed more in the loaded group. Western blot analysis further confirmed that the production of Col I, Runx2 and OPN proteins was significantly higher in the loaded group at 7 days (**Figure 7D**).

***In vivo* bone formation capacity**

The critical calvarial defect is used to evaluate *in vivo* bone formation capacity of cell sheets after mechanical stimulation. After implantation for 4 weeks and 8 weeks, new bone formation is analysed by micro-CT and H&E staining (**Figure 8**). At 4 weeks, as shown in the micro-CT results (**Figure 8A** and **B**), loaded group exhibited better bone formation ability with higher bone volume/tissue volume value in comparison to control and static groups. At 8 weeks, notable new bone formation was observed in the loaded group. In contrast, less new bone tissue was observed at the peripheral part of the

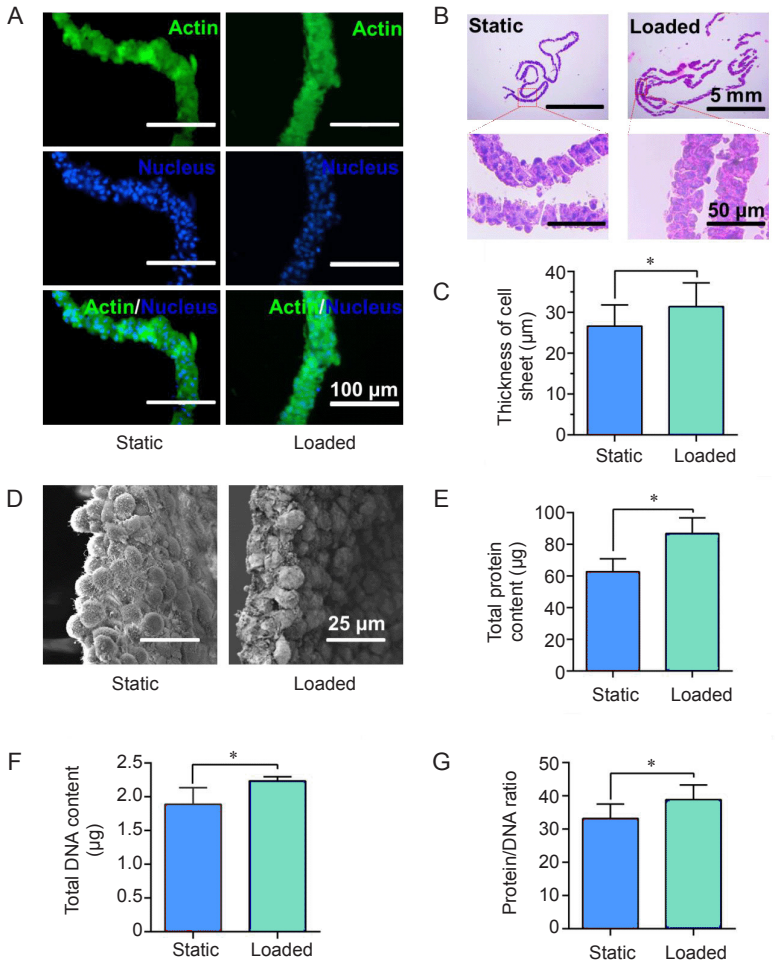


**Figure 6.** Thickness of cell sheets and extracellular matrix production under static and loaded conditions. (A, B) Cytoskeleton staining images (A) and hematoxylin and eosin staining images (B) of cell sheet sections. (C) Statistical analysis of the cell sheet thickness. (D–G) Scanning electron microscope images (D), the total protein contents (E), the total DNA contents (F) and the content ratio of protein to DNA of cell sheets (G) after culturing for 7 days. Scale bars: 100 μm (A), 5 mm (B upper), 50 μm (B lower), 25 μm (C). Data are expressed as the mean ± SD ($n$ = 3). *$P$ < 0.05 (Student's $t$-test).

defects in static and control groups (**Figure 8A**). Moreover, the loaded group showed the highest bone volume/tissue volume value (**Figure 8B**). H&E staining showed that the loaded group had much more new bone formation than the control group and the group with cell sheets alone (**Figure 8C**). The most obvious calcium deposition was observed in the loaded group at 8 weeks, and the newly formed bone in this group began to grow from the periphery to the middle.

## Discussion

As a scaffold-free method, cell sheet engineering provides a promising approach to bone tissue engineering by avoiding scaffold-associated issues like insufficient cell adhesion, probable immune rejection and so on. Generally, the most widely used substrate for cell sheet culturing is rigid culture dish grafted with thermal responsive PNIPAAm and the intact cell sheet is harvested by lowering the temperature. However, except for integrity, thickness, toughness and abundant ECM are important for the application of cell sheets as well. Therefore, in this study, we aim to introduce mechanical stimulation to promote ECM production and bone formation potential of cell sheets.

At present, the most established technology for the preparation of PNIPAAm thermosensitive surface is based on the polymerization initiated by electron beam.[29] However, electron beam irradiation requires expensive equipment. Hence, as an alternative to electron beam radiation, UV radiation was widely used to graft PNIPAAm onto surfaces.[61] Most cell sheets were currently cultivated on solely PNIPAAm-grafted cell culture dishes. Additional treatments are required in terms of different targeted tissues. E.g., patterned surfaces are developed in order to generate heterotypic tissues,[62] and in order to generate more ECM, mechanical stimulation is applied.[63] However, conventional substrates are generally stiff and unstretchable, elastic and stretchable PDMS substrates are admirable to apply mechanical stimulation. The stiffness can also influence cell mechanobiological behaviours, such as cell adhesion, proliferation, and differentiation.[64] In a previous study, elastic PDMS substrates have been grafted with thermal

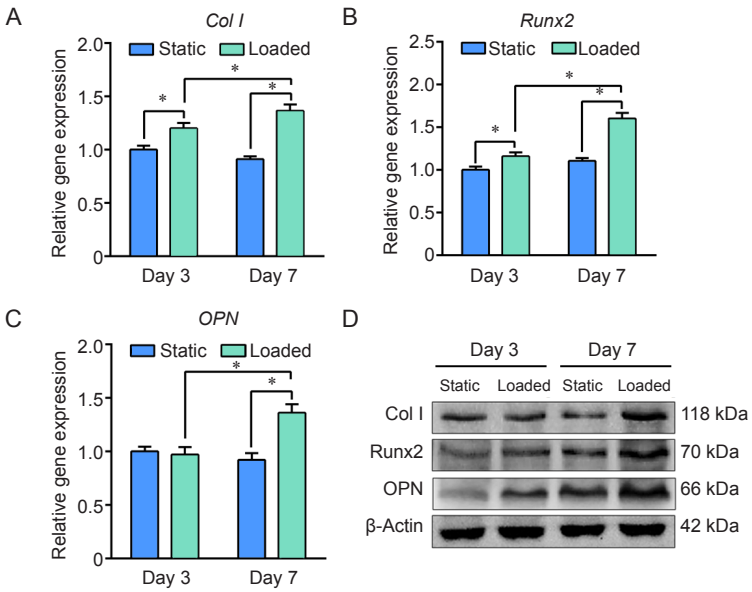


**Figure 7.** Effect of mechanical stimulation on the osteogenesis of MC3T3-E1 cells. (A–C) Gene expression of type I collagen (*Col I*), Runt-related transcription factor 2 (*Runx2*) and osteopontin (*OPN*) using β-actin as housekeeping gene and the static group as control. Data are expressed as the mean ± SD ($n = 3$). *$P < 0.05$ (Student's *t*-test). (D) Western blot analysis of Col I, Runx2 and OPN protein expression.

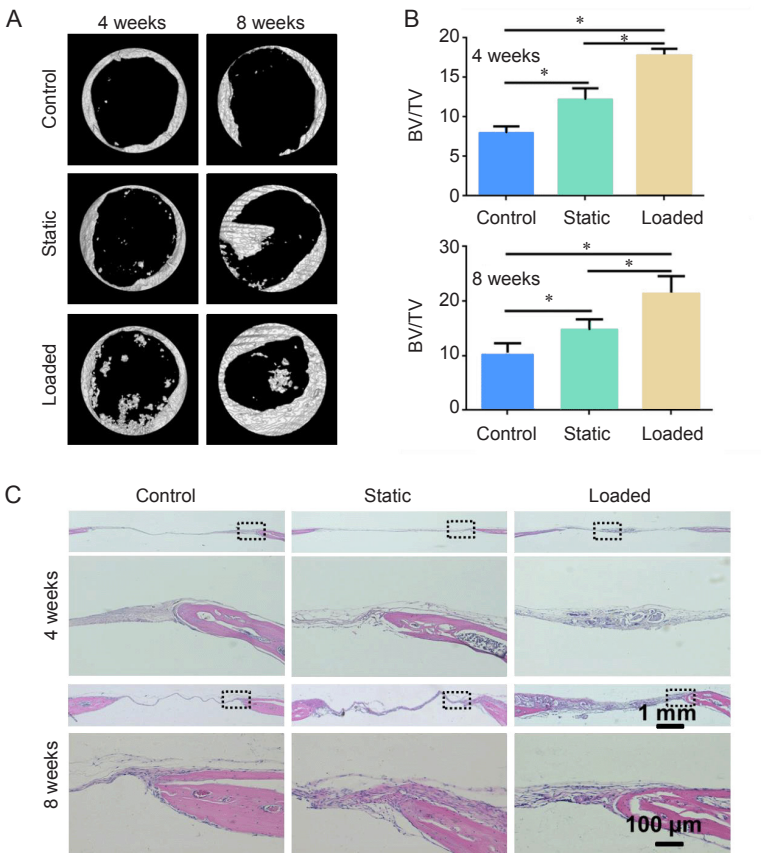


**Figure 8.** Bone formation of cell sheets in the calvarial defects of mice at 4 and 8 weeks, respectively. (A) Three-dimensional reconstruction images. (B) BV/TV at 4 and 8 weeks. Data are expressed as the mean ± SD ($n = 4$). *$P < 0.05$ (one-way analysis of variance followed by Tukey's *post hoc* analysis). (C) Overview and magnified images of the sections stained with hematoxylin and eosin. Scale bars: 1 mm, 100 μm (enlarged images). BV/TV: bone volume/tissue volume.

responsive PNIPAAm by adsorption of photo-initiator and subsequent initiation of grafting polymerization by UV radiation.[65] In this study, PDMS-g-PNIPAAm was prepared by UV-initiated polymerization. The results showed that PDMS-g-PNIPAAm substrates changed from 70° to 50° when the temperature lowered from above 37°C to 4°C (**Figure 3A** and **B**), and the more significant change was found for the substrate with the highest grafting yield, due to more PNIPAAm on the substrates, which makes them the most suitable for cell sheet detachment.

The surface properties of substrates were reported to significantly affect the cell behaviours. For example, fibroblasts spread and proliferate better on PDMS with lower PNIPAAm-grafted yield when treated with gelatin coating, while osteoblasts and mesenchymal stem cells proliferate better on surfaces with higher grafting yields and no gelatin coating.[65, 66] The PNIPAAm-grafted yield was also shown to affect cell detachment.[65] Therefore, cell behaviour on different PDMS-g-PNIPAAm substrates was studied by culturing MC3T3-E1 cells on the substrates. For all the substrates, we found cells could attach and proliferate well on all the substrates without significant differences. However, cell sheets showed different detachment behaviour on PDMS-g-PNIPAAm substrates. For the ones with high grafting yield, the cell sheets could easily detach from the substrate and remain intact after detachment (**Figure 3C**). As mentioned above, substrates with high grafting yield are more sensitive to temperature and more helpful for cell detachment. Our results are in agreement with previous reports on the impacts of grafting yields of PNIPAAm on the detachment behaviour of cell sheets.[67] Therefore, in the following studies, we used the substrates with high grafting yields for their favourable cell detachment behaviour.

Except for the integrity of cell sheets, thickness, toughness and abundant ECM is also important for bone repair. Recently, numerous studies demonstrated the critical impacts of mechanical loading on cell-ECM interactions and ECM formation, in addition to the chemical composition and structure of ECM.[68] Therefore, we hypothesised that cell sheets with enhanced ECM content and strength could be achieved by applying dynamic mechanical stimulation during culturing. The elasticity of PDMS-g-PNIPAAm substrates allows dynamic mechanical stimulation by cyclic stretching of the elastic substrates during cell sheet culturing. Previous work in our laboratory showed that mechanical stretching with the condition of 5% strength, 0.5 Hz, and 4 hours/day, could promote the secretion of ECM and expression of osteogenic-specific genes. The results showed the enhanced thickness for the cell sheets cultured under loaded condition than static condition (**Figure 6A–C** and **Additional Figure 3**). Furthermore, cell sheets cultured under loaded condition seemed to show more cell-to-cell junction and denser ECM (**Figure 6D**). The total protein weight of cell sheet cultured under loaded condition was much higher than static condition (**Figure 6E**). These results indicate that more ECM was formed in the cell sheets after mechanical stimulation. This is in accordance with previous report,[68] showing appropriate mechanical stimulation significantly promotes cell proliferation and ECM secretion.

Several studies have indicated that the expression of various genes in cells could be regulated by applying mechanical stimulations.[43, 49] With hydrostatic pressure and uniaxial compression, MSCs showed enhanced chondrogenic expression, while application of tensile strain enhanced osteogenic expression.[44] The effects of cyclic mechanical stretching on osteogenic differentiation of human intraoral MSCs and expression of osteogenic genes in MC3T3-E1 osteoblasts cells were investigated. The results show that mechanical stimulation can significantly increase osteogenic gene expression and bone formation.[69] In this study, a significant up-regulation of the osteogenic differentiation markers genes *Col I*, *Runx2*, and *OPN* was observed in cell sheets cultured under mechanical stimulation, compared with that cultured under static conditions (**Figure 7**). The higher expression levels of Col I and OPN indicate a higher level of calcification stage. Even single mechanical stimulation up-regulated osteogenic transcription factor Runx2, both in the reverse transcription quantitative polymerase chain reaction and western blot. This over-expression of the transcription factor in mechanically stimulated groups provides evidence that stimulation by cyclic strain promoted MC3T3-E1 differentiation. It has also reported that dynamic stretching of the substrate can cause fluid-induced wall shear stress on cells,[70, 71] which could influence osteogenesis.[72] From our point of view, there might be some wall shear stress at a low level, but the major effect of mechanical-induced osteogenesis is due to mechanical strain. Finally, *in vivo* experiment further indicated the cell sheets prepared under mechanical stimulation had superior bone formation capacity as well (**Figure 8**). In all, we showed that cyclic mechanical stimulation could significantly up-regulate the expression of osteogenic genes, *Col I*, *Runx2*, and *OPN*, and thereby stimulate the differentiation of MC3T3-E1 and further bone formation. Compared to other scaffolds, our scaffold-free cell sheets not only avoid the inflammation caused by degradation of scaffolds and mismatch of cell proliferation, but also generate abundant ECM by applying mechanical stimulation to cells. This study indicates the great potential of mechanically conditioned cell sheets to be used as synthetic bone graft substitutes. The effects of different types and magnitude of the forces on the cell sheets preparation need to be further investigated.

In this study, we successfully prepared a thermal responsive and elastic PDMS-g-PNIPAAm substrate by grafting PNIPAAm on elastomeric using $O_2$-plasma-UV initiated graft polymerization, to study the effects of cyclic mechanical stimulation on cell sheets engineering. MC3T3-E1 cells proliferated well on PDMS-g-PNIPAAm substrates, and intact cell sheets could be easily harvested by lowering the temperature from PDMS-g-PNIPAAm substrates with the highest grafting yield. Cell culture experiment demonstrated that the thickness and the ECM content of cell sheets were remarkably enhanced with mechanical stimulation, and the expression of osteogenic genes and bone formation were significantly promoted. This provides a feasible and facile approach to enhance the properties of engineered cell sheets, and can be further applied with cell sheet engineering techniques for potential scaffold-free tissue engineering applications.

**Author contributions**

BL and SC conceived and designed the study; GW, ZY, LY, YY, PZ, GC, HW, QG, CZ, and FH performed the experiments and data analysis; GW, ZY, LY, SC and BL wrote the manuscript with input from all coauthors. All authors have read and approved the final version of the manuscript.

**Financial support**

This work was financial supported bythe National Natural Science Foundation of China (No. 81925027), and the Priority Academic Program Development of Jiangsu Higher Education Institutions.

**Acknowledgement**

None.

**Conflicts of interest statement**

The authors declare that no competing interests exist.

Editor note: Bin Li is an Editorial Board member of *Biomaterials Translational*. He was blinded from reviewing or making decisions on the manuscript. The article was subject to the journal's standard procedures, with peer review handled independently of this Editorial Board member and his research group.



**Additional files**

***Additional Figure 1:*** Effect of NIPAAm monomer concentration, polymerization temperature, polymerization time and distance from UV source on grafting yield of PDMS-g-PNIPAAm surface.

***Additional Figure 2:*** Energy dispersion spectrum of PDMS, gPDMS-L, gPDMS-M and gPDMS-H substrates.

***Additional Figure 3:*** Masson staining of cell sheet cross-sections and thickness distribution of cell sheet obtained under static or loaded conditions.

1. Green, J. J.; Elisseeff, J. H. Mimicking biological functionality with polymers for biomedical applications. *Nature*. **2016**, *540*, 386-394.
2. Triffitt, J. T.; Wang, Q. Application of stem cells in translational medicine. *Biomater Transl*. **2021**, *2*, 285-286.
3. Steijvers, E.; Ghei, A.; Xia, Z. Manufacturing artificial bone allografts: a perspective. *Biomater Transl*. **2022**, *3*, 65-80.
4. Han, F.; Hu, Y.; Li, J.; Gong, J.; Guo, Q.; Zhu, C.; Zhu, X.; Yang, H.; Li, B. In situ silk fibroin-mediated crystal formation of octacalcium phosphate and its application in bone repair. *Mater Sci Eng C Mater Biol Appl*. **2019**, *95*, 1-10.
5. Burg, K. J.; Porter, S.; Kellam, J. F. Biomaterial developments for bone tissue engineering. *Biomaterials*. **2000**, *21*, 2347-2359.
6. Zhang, K.; Wang, S.; Zhou, C.; Cheng, L.; Gao, X.; Xie, X.; Sun, J.; Wang, H.; Weir, M. D.; Reynolds, M. A.; Zhang, N.; Bai, Y.; Xu, H. H. K. Advanced smart biomaterials and constructs for hard tissue engineering and regeneration. *Bone Res*. **2018**, *6*, 31.
7. Xu, Y.; Peng, J.; Richards, G.; Lu, S.; Eglin, D. Optimization of electrospray fabrication of stem cell-embedded alginate-gelatin microspheres and their assembly in 3D-printed poly(ε-caprolactone) scaffold for cartilage tissue engineering. *J Orthop Translat*. **2019**, *18*, 128-141.
8. Rafat, M.; Li, F.; Fagerholm, P.; Lagali, N. S.; Watsky, M. A.; Munger, R.; Matsuura, T.; Griffith, M. PEG-stabilized carbodiimide crosslinked collagen-chitosan hydrogels for corneal tissue engineering. *Biomaterials*. **2008**, *29*, 3960-3972.
9. Kumbar, S. G.; Nukavarapu, S. P.; James, R.; Nair, L. S.; Laurencin, C. T. Electrospun poly(lactic acid-co-glycolic acid) scaffolds for skin tissue engineering. *Biomaterials*. **2008**, *29*, 4100-4107.
10. Chouhan, D.; Mandal, B. B. Silk biomaterials in wound healing and skin regeneration therapeutics: from bench to bedside. *Acta Biomater*. **2020**, *103*, 24-51.
11. Xuan, H.; Hu, H.; Geng, C.; Song, J.; Shen, Y.; Lei, D.; Guan, Q.; Zhao, S.; You, Z. Biofunctionalized chondrogenic shape-memory ternary scaffolds for efficient cell-free cartilage regeneration. *Acta Biomater*. **2020**, *105*, 97-110.
12. Castilho, M.; Mouser, V.; Chen, M.; Malda, J.; Ito, K. Bi-layered micro-fibre reinforced hydrogels for articular cartilage regeneration. *Acta Biomater*. **2019**, *95*, 297-306.
13. Bhatia, S. N.; Underhill, G. H.; Zaret, K. S.; Fox, I. J. Cell and tissue engineering for liver disease. *Sci Transl Med*. **2014**, *6*, 245sr242.
14. Sabetkish, S.; Kajbafzadeh, A. M.; Sabetkish, N.; Khorramirouz, R.; Akbarzadeh, A.; Seyedian, S. L.; Pasalar, P.; Orangian, S.; Beigi, R. S.; Aryan, Z.; Akbari, H.; Tavangar, S. M. Whole-organ tissue engineering: decellularization and recellularization of three-dimensional matrix liver scaffolds. *J Biomed Mater Res A*. **2015**, *103*, 1498-1508.
15. Shimizu, T.; Yamato, M.; Kikuchi, A.; Okano, T. Cell sheet engineering for myocardial tissue reconstruction. *Biomaterials*. **2003**, *24*, 2309-2316.
16. Qazi, T. H.; Mooney, D. J.; Pumberger, M.; Geissler, S.; Duda, G. N. Biomaterials based strategies for skeletal muscle tissue engineering: existing technologies and future trends. *Biomaterials*. **2015**, *53*, 502-521.
17. Pedde, R. D.; Mirani, B.; Navaei, A.; Styan, T.; Wong, S.; Mehrali, M.; Thakur, A.; Mohtaram, N. K.; Bayati, A.; Dolatshahi-Pirouz, A.; Nikkhah, M.; Willerth, S. M.; Akbari, M. Emerging biofabrication strategies for engineering complex tissue constructs. *Adv Mater*. **2017**, *29*, 1606061.
18. Yang, J.; Yamato, M.; Kohno, C.; Nishimoto, A.; Sekine, H.; Fukai, F.; Okano, T. Cell sheet engineering: recreating tissues without biodegradable scaffolds. *Biomaterials*. **2005**, *26*, 6415-6422.
19. Yamato, M.; Okano, T. Cell sheet engineering. *Mater Today*. **2004**, *7*, 42-47.
20. Xu, X.; Song, J. Segmental long bone regeneration guided by degradable synthetic polymeric scaffolds. *Biomater Transl*. **2020**, *1*, 33-45.
21. McMurray, R. J.; Gadegaard, N.; Tsimbouri, P. M.; Burgess, K. V.; McNamara, L. E.; Tare, R.; Murawski, K.; Kingham, E.; Oreffo, R. O.; Dalby, M. J. Nanoscale surfaces for the long-term maintenance of mesenchymal stem cell phenotype and multipotency. *Nat Mater*. **2011**, *10*, 637-644.
22. Kelm, J. M.; Fussenegger, M. Scaffold-free cell delivery for use in regenerative medicine. *Adv Drug Deliv Rev*. **2010**, *62*, 753-764.
23. Badylak, S. F.; Gilbert, T. W. Immune response to biologic scaffold materials. *Semin Immunol*. **2008**, *20*, 109-116.
24. Anderson, J. M.; Rodriguez, A.; Chang, D. T. Foreign body reaction to biomaterials. *Semin Immunol*. **2008**, *20*, 86-100.
25. Akizuki, T.; Oda, S.; Komaki, M.; Tsuchioka, H.; Kawakatsu, N.; Kikuchi, A.; Yamato, M.; Okano, T.; Ishikawa, I. Application of periodontal ligament cell sheet for periodontal regeneration: a pilot study in beagle dogs. *J Periodontal Res*. **2005**, *40*, 245-251.
26. L'Heureux, N.; Dusserre, N.; Konig, G.; Victor, B.; Keire, P.; Wight, T. N.; Chronos, N. A.; Kyles, A. E.; Gregory, C. R.; Hoyt, G.; Robbins, R. C.; McAllister, T. N. Human tissue-engineered blood vessels for adult arterial revascularization. *Nat Med*. **2006**, *12*, 361-365.
27. Nishida, K.; Yamato, M.; Hayashida, Y.; Watanabe, K.; Maeda, N.; Watanabe, H.; Yamamoto, K.; Nagai, S.; Kikuchi, A.; Tano, Y.; Okano, T. Functional bioengineered corneal epithelial sheet grafts from corneal stem cells expanded ex vivo on a temperature-responsive cell culture surface. *Transplantation*. **2004**, *77*, 379-385.
28. Matsuura, K.; Masuda, S.; Haraguchi, Y.; Yasuda, N.; Shimizu, T.; Hagiwara, N.; Zandstra, P. W.; Okano, T. Creation of mouse embryonic stem cell-derived cardiac cell sheets. *Biomaterials*. **2011**, *32*, 7355-7362.

29. Doberenz, F.; Zeng, K.; Willems, C.; Zhang, K.; Groth, T. Thermoresponsive polymers and their biomedical application in tissue engineering - a review. *J Mater Chem B.* **2020**, *8*, 607-628.
30. Yamato, M.; Utsumi, M.; Kushida, A.; Konno, C.; Kikuchi, A.; Okano, T. Thermo-responsive culture dishes allow the intact harvest of multilayered keratinocyte sheets without dispase by reducing temperature. *Tissue Eng.* **2001**, *7*, 473-480.
31. Lin, J. B.; Isenberg, B. C.; Shen, Y.; Schorsch, K.; Sazonova, O. V.; Wong, J. Y. Thermo-responsive poly(N-isopropylacrylamide) grafted onto microtextured poly(dimethylsiloxane) for aligned cell sheet engineering. *Colloids Surf B Biointerfaces.* **2012**, *99*, 108-115.
32. Yu, Q.; Zhang, Y.; Chen, H.; Zhou, F.; Wu, Z.; Huang, H.; Brash, J. L. Protein adsorption and cell adhesion/detachment behavior on dual-responsive silicon surfaces modified with poly(N-isopropylacrylamide)-block-polystyrene copolymer. *Langmuir.* **2010**, *26*, 8582-8588.
33. Kushida, A.; Yamato, M.; Konno, C.; Kikuchi, A.; Sakurai, Y.; Okano, T. Decrease in culture temperature releases monolayer endothelial cell sheets together with deposited fibronectin matrix from temperature-responsive culture surfaces. *J Biomed Mater Res.* **1999**, *45*, 355-362.
34. Hamdi, H.; Furuta, A.; Bellamy, V.; Bel, A.; Puymirat, E.; Peyrard, S.; Agbulut, O.; Menasché, P. Cell delivery: intramyocardial injections or epicardial deposition? A head-to-head comparison. *Ann Thorac Surg.* **2009**, *87*, 1196-1203.
35. Shimizu, T.; Sekine, H.; Yang, J.; Isoi, Y.; Yamato, M.; Kikuchi, A.; Kobayashi, E.; Okano, T. Polysurgery of cell sheet grafts overcomes diffusion limits to produce thick, vascularized myocardial tissues. *FASEB J.* **2006**, *20*, 708-710.
36. Liu, Y.; Wang, L.; Li, S.; Zhang, T.; Chen, C.; Hu, J.; Sun, D.; Lu, H. Mechanical stimulation improves rotator cuff tendon-bone healing via activating IL-4/JAK/STAT signaling pathway mediated macrophage M2 polarization. *J Orthop Translat.* **2022**, *37*, 78-88.
37. Lin, C. Y.; Song, X.; Seaman, K.; You, L. Microfluidic co-culture platforms for studying osteocyte regulation of other cell types under dynamic mechanical stimulation. *Curr Osteoporos Rep.* **2022**, *20*, 478-492.
38. Zhang, J.; Hao, X.; Chi, R.; Qi, J.; Xu, T. Moderate mechanical stress suppresses the IL-1β-induced chondrocyte apoptosis by regulating mitochondrial dynamics. *J Cell Physiol.* **2021**, *236*, 7504-7515.
39. Lee, H. P.; Gu, L.; Mooney, D. J.; Levenston, M. E.; Chaudhuri, O. Mechanical confinement regulates cartilage matrix formation by chondrocytes. *Nat Mater.* **2017**, *16*, 1243-1251.
40. Wang, T.; Chen, P.; Chen, L.; Zhou, Y.; Wang, A.; Zheng, Q.; Mitchell, C. A.; Leys, T.; Tuan, R. S.; Zheng, M. H. Reduction of mechanical loading in tendons induces heterotopic ossification and activation of the β-catenin signaling pathway. *J Orthop Translat.* **2021**, *29*, 42-50.
41. Guilak, F. Biomechanical factors in osteoarthritis. *Best Pract Res Clin Rheumatol.* **2011**, *25*, 815-823.
42. Ni, R.; Guo, X. E.; Yan, C.; Wen, C. Hemodynamic stress shapes subchondral bone in osteoarthritis: An emerging hypothesis. *J Orthop Translat.* **2022**, *32*, 85-90.
43. Gauvin, R.; Parenteau-Bareil, R.; Larouche, D.; Marcoux, H.; Bisson, F.; Bonnet, A.; Auger, F. A.; Bolduc, S.; Germain, L. Dynamic mechanical stimulations induce anisotropy and improve the tensile properties of engineered tissues produced without exogenous scaffolding. *Acta Biomater.* **2011**, *7*, 3294-3301.
44. Dai, Z. Q.; Wang, R.; Ling, S. K.; Wan, Y. M.; Li, Y. H. Simulated microgravity inhibits the proliferation and osteogenesis of rat bone marrow mesenchymal stem cells. *Cell Prolif.* **2007**, *40*, 671-684.
45. Vandenburgh, H. H. Dynamic mechanical orientation of skeletal myofibers in vitro. *Dev Biol.* **1982**, *93*, 438-443.
46. Vandenburgh, H. H.; Swasdison, S.; Karlisch, P. Computer-aided mechanogenesis of skeletal muscle organs from single cells in vitro. *FASEB J.* **1991**, *5*, 2860-2867.
47. Collinsworth, A. M.; Torgan, C. E.; Nagda, S. N.; Rajalingam, R. J.; Kraus, W. E.; Truskey, G. A. Orientation and length of mammalian skeletal myocytes in response to a unidirectional stretch. *Cell Tissue Res.* **2000**, *302*, 243-251.
48. Hu, B.; El Haj, A. J.; Dobson, J. Receptor-targeted, magneto-mechanical stimulation of osteogenic differentiation of human bone marrow-derived mesenchymal stem cells. *Int J Mol Sci.* **2013**, *14*, 19276-19293.
49. Lambert, C. A.; Colige, A. C.; Munaut, C.; Lapière, C. M.; Nusgens, B. V. Distinct pathways in the over-expression of matrix metalloproteinases in human fibroblasts by relaxation of mechanical tension. *Matrix Biol.* **2001**, *20*, 397-408.
50. Gilbert, T. W.; Stewart-Akers, A. M.; Sydeski, J.; Nguyen, T. D.; Badylak, S. F.; Woo, S. L. Gene expression by fibroblasts seeded on small intestinal submucosa and subjected to cyclic stretching. *Tissue Eng.* **2007**, *13*, 1313-1323.
51. Ducouret, C.; Petersohn, E.; Betz, N.; Le Moel, A. Fourier transform infrared analysis of heavy ion grafting of poly(vinylidene fluoride). *Spectrochim Acta A Mol Biomol Spectrosc.* **1995**, *51*, 567-572.
52. Ponomar, M.; Krasnyuk, E.; Butylskii, D.; Nikonenko, V.; Wang, Y.; Jiang, C.; Xu, T.; Pismenskaya, N. Sessile drop method: critical analysis and optimization for measuring the contact angle of an ion-exchange membrane surface. *Membranes (Basel).* **2022**, *12*, 765.
53. Huhtamäki, T.; Tian, X.; Korhonen, J. T.; Ras, R. H. A. Surface-wetting characterization using contact-angle measurements. *Nat Protoc.* **2018**, *13*, 1521-1538.
54. Schneider, C. A.; Rasband, W. S.; Eliceiri, K. W. NIH Image to ImageJ: 25 years of image analysis. *Nat Methods.* **2012**, *9*, 671-675.
55. Yu, L.; Cai, Y.; Wang, H.; Pan, L.; Li, J.; Chen, S.; Liu, Z.; Han, F.; Li, B. Biomimetic bone regeneration using angle-ply collagen membrane-supported cell sheets subjected to mechanical conditioning. *Acta Biomater.* **2020**, *112*, 75-86.
56. Zhang, W.; Wang, H.; Yuan, Z.; Chu, G.; Sun, H.; Yu, Z.; Liang, H.; Liu, T.; Zhou, F.; Li, B. Moderate mechanical stimulation rescues degenerative annulus fibrosus by suppressing caveolin-1 mediated pro-inflammatory signaling pathway. *Int J Biol Sci.* **2021**, *17*, 1395-1412.
57. Livak, K. J.; Schmittgen, T. D. Analysis of relative gene expression data using real-time quantitative PCR and the 2(-Delta Delta C(T)) method. *Methods.* **2001**, *25*, 402-408.
58. National Research Council. Guide for the Care and Use of Laboratory Animals, 8th edition. National Academies Press: Washington, DC, USA, 2011.
59. Liu, L.; Sheardown, H. Glucose permeable poly (dimethyl siloxane) poly (N-isopropyl acrylamide) interpenetrating networks as ophthalmic biomaterials. *Biomaterials.* **2005**, *26*, 233-244.
60. Huang, X.; Das, R.; Patel, A.; Nguyen, T. D. Physical stimulations for bone and cartilage regeneration. *Regen Eng Transl Med.* **2018**, *4*, 216-237.
61. Sugiura, S.; Imano, W.; Takagi, T.; Sakai, K.; Kanamori, T. Thermoresponsive protein adsorption of poly(N-isopropylacrylamide)-modified streptavidin on polydimethylsiloxane microchannel surfaces. *Biosens Bioelectron.* **2009**, *24*, 1135-1140.
62. Rim, N. G.; Yih, A.; Hsi, P.; Wang, Y.; Zhang, Y.; Wong, J. Y. Micropatterned cell sheets as structural building blocks for biomimetic vascular patches. *Biomaterials.* **2018**, *181*, 126-139.
63. Kessler, D.; Dethlefsen, S.; Haase, I.; Plomann, M.; Hirche, F.; Krieg, T.;

Eckes, B. Fibroblasts in mechanically stressed collagen lattices assume a "synthetic" phenotype. *J Biol Chem.* **2001**, *276*, 36575-36585.
64. Zhang, W.; Chu, G.; Wang, H.; Chen, S.; Li, B.; Han, F. Effects of matrix stiffness on the differentiation of multipotent stem cells. *Curr Stem Cell Res Ther.* **2020**, *15*, 449-461.
65. Ma, D.; Chen, H.; Shi, D.; Li, Z.; Wang, J. Preparation and characterization of thermo-responsive PDMS surfaces grafted with poly(N-isopropylacrylamide) by benzophenone-initiated photopolymerization. *J Colloid Interface Sci.* **2009**, *332*, 85-90.
66. Shi, D.; Ma, D.; Dong, F.; Zong, C.; Liu, L.; Shen, D.; Yuan, W.; Tong, X.; Chen, H.; Wang, J. Proliferation and multi-differentiation potentials of human mesenchymal stem cells on thermoresponsive PDMS surfaces grafted with PNIPAAm. *Biosci Rep.* **2009**, *30*, 149-158.
67. Nagase, K.; Yamato, M.; Kanazawa, H.; Okano, T. Poly(N-isopropylacrylamide)-based thermoresponsive surfaces provide new types of biomedical applications. *Biomaterials.* **2018**, *153*, 27-48.
68. Humphrey, J. D.; Dufresne, E. R.; Schwartz, M. A. Mechanotransduction and extracellular matrix homeostasis. *Nat Rev Mol Cell Biol.* **2014**, *15*, 802-812.
69. Hao, J.; Zhang, Y.; Jing, D.; Shen, Y.; Tang, G.; Huang, S.; Zhao, Z. Mechanobiology of mesenchymal stem cells: Perspective into mechanical induction of MSC fate. *Acta Biomater.* **2015**, *20*, 1-9.
70. Kreutzer, J.; Viehrig, M.; Pölönen, R. P.; Zhao, F.; Ojala, M.; Aalto-Setälä, K.; Kallio, P. Pneumatic unidirectional cell stretching device for mechanobiological studies of cardiomyocytes. *Biomech Model Mechanobiol.* **2020**, *19*, 291-303.
71. Thompson, M. S.; Abercrombie, S. R.; Ott, C. E.; Bieler, F. H.; Duda, G. N.; Ventikos, Y. Quantification and significance of fluid shear stress field in biaxial cell stretching device. *Biomech Model Mechanobiol.* **2011**, *10*, 559-564.
72. Wittkowske, C.; Reilly, G. C.; Lacroix, D.; Perrault, C. M. In vitro bone cell models: impact of fluid shear stress on bone formation. *Front Bioeng Biotechnol.* **2016**, *4*, 87.

Received: November 24, 2022
Revised: January 14, 2023
Accepted: February 17, 2023
Available online: March 28, 2023